LETTERS
PUBLISHED ONLINE: 26 SEPTEMBER 2010 | DOI: 10.1038/NGEO969
nature geoscience

Seismic evidence for a global low-velocity layer within the Earth's upper mantle

Benoît Tauzin[1]*, Eric Debayle[2] and Gérard Wittlinger[3]

Within the upper mantle, the seismic discontinuity at 410-km depth marks the top of the transition zone and is attributed to pressure-induced transformation of olivine into wadsleyite mineral assemblage. Just above the 410-km discontinuity, a layer characterized by low seismic wave velocities has been identified regionally[1,2]. This low velocity layer shows poor lateral continuity and is thought to represent partial melting induced by local effects, such as the dehydration of subducted crust[1] or the dehydration of water-bearing silicates beneath continental platforms in association with mantle plumes[2]. However, some models predict that the low-velocity layer should extend globally, because the weaker water storage capacity of upper mantle minerals should induce partial melting of water-bearing silicates throughout this region[3,4]. Here we report seismic observations from 89 stations worldwide that indicate a thick, intermittent low-velocity layer is located near 350 km depth in the mantle. The low velocity layer is not limited to regions associated with subduction or mantle plumes, and shows no affinity to a particular tectonic environment. We suggest that our data image the thickest parts of a more continuous global structure that shows steep lateral variations in thickness. The presence of a global layer of partial melt above the 410-km discontinuity would modify material circulation in the Earth mantle and may help to reconcile geophysical and geochemical observations[3].

Recent experimental results indicate that melting may occur in the deep upper mantle or transition zone[5,6] and melt could be neutrally buoyant in the high pressure conditions at the top of the mantle transition zone[7,8]. If partial melt is sequestered atop the 410-km ('410') discontinuity, it is expected to reduce seismic velocities within a low velocity layer (LVL).

Previous reports of a such a LVL have been studies[1,9–19] focused on particular regions of the world. The only exception is a global study of the LVL based on S-to-P (Sp) conversions[2]. In that study, an LVL was found under eleven seismic stations spread across Africa, Asia and Antarctica. These observations remain very sparse (Supplementary Fig. S1) and thus the presence of melt over large areas is unknown.

We built a P-to-S (Ps) conversion database designed to investigate, by improving its global sampling, whether the LVL atop the '410' has a global character. We take advantage of the fact that Ps conversions are observed over a greater range of epicentral distances than Sp conversions. Furthermore, contrary to Sp with SKS, Ps phases do not suffer from interference with other main seismic arrivals. This allows us to improve the signal to noise ratio by stacking (see Methods section) a larger number of receiver functions (RFs) at many more stations. However, in the 300–400 km depth range, a careful analysis is needed to avoid multiple reverberations in the Ps signal. In this study, the data are first processed in the 7–75 s period range to minimize microseismic noise. The entire data set is then reprocessed in three other period ranges (3–75 s, 5–75 s and 10–75 s). This multiple frequency approach allows us to ensure that LVL signals are not artefacts introduced during signal processing (see Methods section).

We start from a global data set of mantle Ps RFs (ref. 20) completed with data recorded at the Mednet and US permanent stations. We discard stations with strong oscillations on the stacked RFs (see Methods section). After a careful visual inspection of the stacked RFs at each station, we select those showing a good waveform agreement with synthetics computed with the IASP91 (ref. 21) velocity model. We also check, using slant-stack diagrams built in the four frequency ranges of analysis, that no ambiguous reverberated arrivals are present around the time expected for the P410s arrival (see Methods section). Our final database consists of 152 globally distributed stations, with a much better global coverage of the LVL than previous Ps or Sp studies[2,10–16].

Our stacked RFs (Fig. 1) show prominent positive amplitude signals associated with steep downward increases of seismic velocities at the Mohorovičić (near 35 km depth) and the 410-km discontinuities. A strong negative amplitude signal (in red in Fig. 1a) is observed near 350 km depth under 89 stations of our data set. At each station, this signal emerges from the noise at the 95% confidence level (see Methods section).

The negative signal seen near 350 km depth (Fig. 1a) is not a side-lobe of the P410s waveform because (1) we do not observe a symmetric side-lobe with a similar amplitude underneath the '410' in the four period ranges of analysis, (2) the distance between the negative signal and the '410' varies with the station location, (3) changing the filter does not change the position of the negative signal (Supplementary Fig. S2), (4) synthetic RFs computed using the IASP91 velocity model do not show spurious side lobes (Fig. 2a) and (5) the negative signal near 350 km depth is very weak or absent under the other 63 stations (Fig. 1b) although the amplitude of the '410' is not significantly different.

The negative signal near 350 km depth is also not a reverberation between the surface and a discontinuity located in the uppermost mantle. First, this signal has a positive slowness, compatible with Ps direct conversions, whereas for multiple reverberations, a negative slowness would be expected (see Methods section). Second, reverberations always show greater depth variations than the original discontinuity (for example $\pm$42 km for the standard deviation of the PpSms + PsPms phase against $\pm$10 km for the Moho standard deviation, Fig. 1a,b). The signal observed near 350 km (Fig. 1a) occurs at an average depth of 354 $\pm$ 24 km. If this signal is produced by multiple reverberations between a discontinuity and the surface, this discontinuity must be present in

[1]Department of Earth Sciences, Utrecht University, PO Box 80.021, 3508 TA Utrecht, The Netherlands, [2]Laboratoire de Sciences de la Terre, Université de Lyon I, CNRS and Ecole Normale Supérieure de Lyon, UMR5570, F-69622 Villeurbanne, France, [3]Ecole et Observatoire des Sciences de la Terre, UMR-CNRS 7516, 5 rue René Descartes, 67084 Strasbourg Cedex, France. *e-mail: benoit@geo.uu.nl.

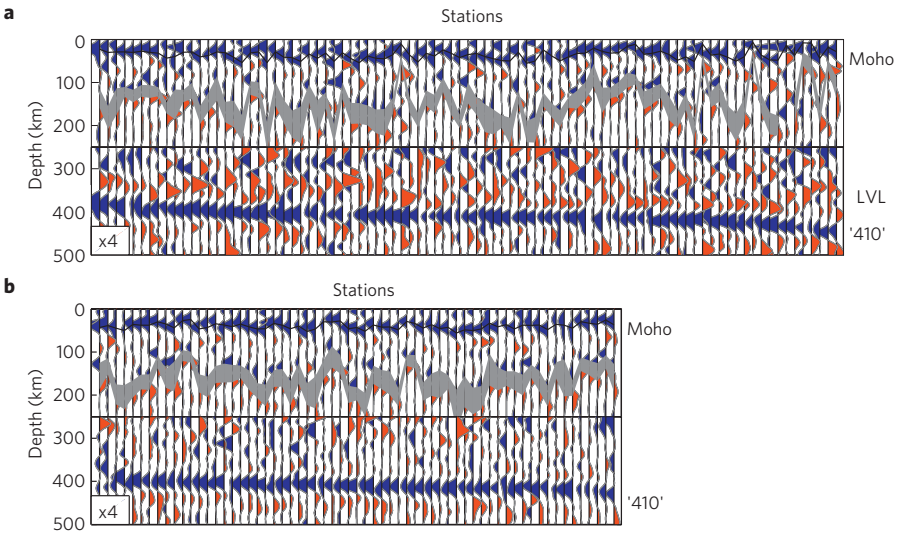

Figure 1 | Signal associated with the mantle structure under individual seismic stations. a, 89 stations show a negative signal atop the '410'. **b**, 63 stations show no clear signal atop the '410'. Blue and red colours indicate positive and negative amplitudes respectively. Amplitudes in the first 250 km have been reduced by a factor 4. Stations are sorted according to the depth of the 410-km discontinuity. The depth of the Mohorovičić discontinuity is marked with a thin black line. The depth interval blurred by the PpPms and PpSms + PsPms reverberations is shaded in grey.

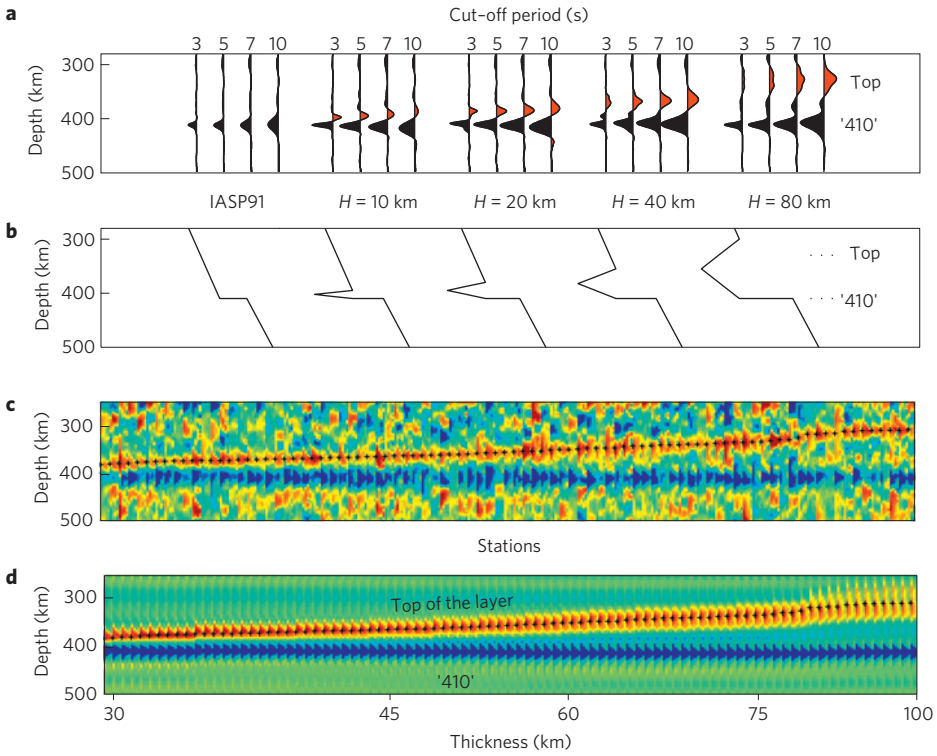

Figure 2 | Modelling the low velocity layer. a,**b**, Synthetic receiver functions (**a**) and associated seismic models (**b**) for different thicknesses H of a LVL atop the '410' (see Methods section). **c**,**d**, Observed RFs (**c**) for the 89 stations of Fig. 1a and synthetic waveforms (**d**) computed using the same LVL thickness distribution as in the data in **c**. Each seismic trace (**c**,**d**) is made of the juxtaposition, from left to right, of the 10, 7, 5 and 3 s low-pass filtered RFs at the stations, aligned on the '410' waveform and ordered by increasing LVL thickness. Black crosses indicate the top of the LVL.

many regions of the world and be remarkably flat. Although several discontinuities have been observed in the uppermost 200 km of the mantle, none of them present such characteristics[22,23].

A signal similar to that observed near 350 km depth in our data was found in regional conversion, reflection and refraction datasets[1,2,9–17] and was associated with a downward negative velocity gradient marking the top of a LVL above the '410' discontinuity. We produced a set of synthetic RFs (Fig. 2a) using the IASP91 velocity model modified with a low velocity layer atop the '410' (Fig. 2b). A trade-off exists between the velocity contrast and the vertical extension of the gradient at the top of the layer[9]. We use constraints from prior studies for both the velocity contrast[2,9,12,13] and the geometry of the layer[2] (see Methods section) and vary the vertical extension of the top gradient (Fig. 2b). Our data do not resolve a LVL thinner than 20 km because the noise level is too high at the shortest periods (Supplementary Fig. S2). However,

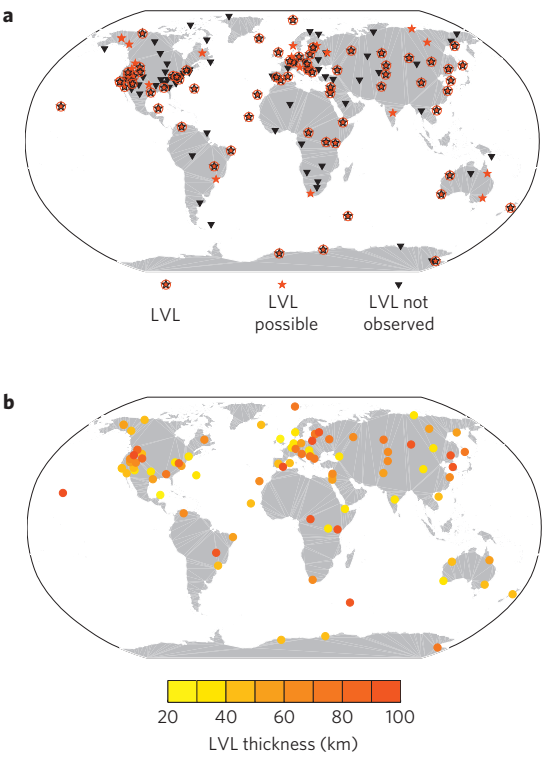

Figure 3 | Mapping the layer atop the 410-km discontinuity. a, Global map of the LVL. Stations where the LVL is detected are shown with red stars. Our strongest observations (see Methods section) are outlined with red circles. Black triangles indicate stations where the LVL is not observed. **b**, Global map of the estimated LVL thickness.

our experiments show that in the range of observable thicknesses (>20 km), a close fit to the observed signal is obtained, assuming a 0.2 km s^{-1} downward shear-wave velocity decrease (Fig. 2c,d).

The LVL is found beneath all continents and, despite a sparse sampling of the oceans, at a few oceanic stations (Fig. 3a and Supplementary Fig. S3). The LVL is not related to a particular type of geodynamical environment atop the '410': it is found below 34 stations located in the vicinity of large igneous provinces (LIPs) or hotspots, below 9 stations located in the vicinity of deep subduction zones and below 46 stations located away from recent volcanism and subduction (Supplementary Figs S4, S5). Also, among the 63 stations where it is not observed, 21 are located near LIPs or hotspots, 7 are in the vicinity of recent subduction zones and 37 are located away from LIPs, hotspots and subduction. Finally, the detection of the LVL is not correlated to a particular subdivision of the lithosphere according to its age[24] (Supplementary Fig. S6).

The LVL thickness varies from ~30 to ~100 km. Variations exceeding 20 km at stations distant by ~200 km are frequent (Fig. 3b). Furthermore, the LVL can disappear over short distances (Fig. 3a), as can be seen in regions where the station coverage is dense, such as North America, Europe and Asia. Short-scale horizontal variations from a thick (>30 km) to a thin layer, undetectable with our data, could explain these differences. Our results can be compared with two previous regional studies of the LVL in the western US (refs 9,15) (see Supplementary Fig. S1). From the dense networks of stations available in this region, the LVL atop the '410' was found to change rapidly in thickness over length scales of about 100–200 km. Our global observations indicate that thickness variations over similar length scales could be present at a global scale.

Our observations indicate a compositional origin for the LVL: lateral variations of the LVL thickness are difficult to reconcile with the effect of temperature alone. Furthermore, there is no correlation between the presence of a LVL and the depth of the '410' (Fig. 1a) or the transition zone thickness, which are supposed to be markers of the temperature. Partial melting is the most probable candidate[1–3,5–9] and can be explained by either high water concentrations, which decrease the solidus temperature of mantle rocks under the Earth geotherm, or anomalously high temperatures exceeding the dry solidus of mantle silicate rocks.

A subset of our observations located in the vicinity of subduction zones may be explained by dehydration, either due to volatile entrainment by subduction[1] to the top of the '410', or to bottom-up water release from a stagnant slab in the mantle transition zone (MTZ; refs 9,17). Another subset could be attributed to the effect of high temperatures on water rich mantle silicate rocks, as has been suggested in previous Sp studies[2,12,13]. Our results, on the basis of a larger sampling of the Earth mantle, indicate however that the LVL is not solely found beneath subduction zones or Precambrian platforms in association with Mesozoic or Cenozoic mantle plumes.

The transition zone water filter (TZWF) model[3,4] predicts the existence of a partial-melt layer atop the '410', extending over great areas, and could explain a greater variety of our observations. In this model, a global diffuse vertical ascendant flow is transmitted to the material of the MTZ to compensate the excess mass penetrating into the deep mantle under the subduction zones. On reaching the pressure condition of the phase transition at 410 km depth, phase transforming and hydrated MTZ minerals would become water saturated or super-saturated as a result of the weaker water storage capacity of the upper mantle minerals[25]. The high water content of the rocks above the '410' would decrease the wet solidus temperature under the Earth geotherm and initiate partial melting even without anomalously high temperatures.

However, this model also predicts a reduced LVL thickness in the vicinity of mantle plumes, due to high ascent velocities or to a thermally induced decrease of the water solubility in MTZ minerals[26]. This reduced thickness is not observed in our data, as we find a 'thick' (>30 km) LVL in the vicinity of several possible mantle plumes (for example, the Afar plume on Fig. 3b).

Our observations of a 'thick' LVL atop the 410-km discontinuity in various regions of the world, including the vicinity of mantle plumes, remain to be explained. Short-scale variations in the LVL thickness indicate a possible lens-type structure with localized thick pockets of partial melt. Our results show that the development of such pockets is not specific to a particular geodynamical environment and seems to be largely controlled by local conditions near the 410-km discontinuity. It is possible that we sample the thickest parts of a global partial melt layer showing rapid variations in thickness. If the melt layer has a global character, it must change global mantle circulation and geochemistry, for instance by filtering incompatible elements[3]. Melt distribution and interconnectivity play an important role in the stability and steady-state thickness of a melt layer[27]. A recent work[28] suggests that grain boundary tension may prevent simple gravitational settling of a heavy melt into a thin completely decompacted layer, and may give rise to a thicker boundary layer. The effect of grain boundary tension is modulated by the grain size and the matrix viscosity, which can vary by orders of magnitude in the Earth mantle. Consequently, the steady state thickness of the dense melt-rich layer will also show substantial variation.

Methods

The receiver functions are time series showing the elastic response to an excitation of the Earth structure beneath the receivers. These RFs are computed from seismograms filtered in four period ranges ([3; 75] s, [5; 75] s, [7; 75] s, [10; 75] s) using a methodology explained in ref. 19. The type of filtering (forward and reverse using linear-phase Butterworth filters) enables us to reduce signal phase distortions on the seismograms. The deconvolution method[20] is chosen to reduce frequency-dependent artefacts (side-lobes) on the RFs. During the deconvolution[20] process, the RFs are normalized so that Ps amplitudes are expressed as a percentage of the P-wave amplitude. At a given station, the RFs are (1) stacked[20] in the time domain and (2) time-to-depth converted[20] using a 3D

shear-wave velocity model[29]. These operations are performed for all stations in the four period ranges of analysis.

Multiple frequency analysis. The dominant period of the Ps waves is smaller than 10 s. Therefore, by decreasing the lower corner period of our Butterworth filter from 10 to 3 s, we should in principle improve the vertical resolution. However, the level of noise also increases (Supplementary Fig. S2). We found the multiple frequency analysis very useful to detect possible multiple reverberations and to cross-check that the LVL signal is not a side lobe of the '410' (Supplementary Fig. S2).

Selection by waveform. We checked by visual inspection that the stacked RFs have no strong signal distortion in comparison to synthetic RFs computed with the IASP91 (ref. 21) velocity model. We show in Supplementary Fig. S7 examples of waveforms consistent with the IASP91 velocity structure at BOSA and ARU stations, and a more complicated and oscillating waveform at MAJO station, which is located near a subduction zone. In general, strongly oscillating RFs in the 20–75 s time window (equivalent to the 200–750 km depth range) are associated with structural complexities in the vicinity of subduction zones and orogenic regions, or are related to the presence of an ice sheet. Stations, such as MAJO, where oscillations could mask a LVL signal are rejected.

Selection by slowness. We built slant-stack diagrams (see Supplementary Fig. S8 and ref. 20) for each station and in the four period ranges of analysis to check that there are no multiple reverberations arriving around the P410s arrival. Such diagrams give constraints on the apparent slowness of waves recorded at the stations. Direct conversions are expected with a positive differential slowness, whereas multiple reverberations are expected with a negative differential slowness. For station Wushi (Supplementary Fig. S8), the negative signal preceding the P410s arrival is probably a direct conversion, as it comes with the right slowness. The negative signal preceding the P410s arrival at Palmer Station (Supplementary Fig. S8) is apparently associated with a multiple reverberation. Stations showing a signal dominated by multiple reverberations, such as PMSA, are discarded.

Noise level and the 350-km depth signal. We look for any significant negative Ps conversion emerging from the noise in the 300 to 410 km depth interval. To measure the noise level, we apply a bootstrap re-sampling approach[30]. At each station, and for each sample t of the stacked RF, we obtain a distribution of amplitude, a mean and a standard deviation $\sigma(t)$. Any amplitude on the stacked data which goes beyond the $\pm 2\sigma(t)$ level (95% confidence level) is considered as emerging from the noise. We give in Supplementary Fig. S7 examples of such waveforms (in grey) for BOSA and ARU stations. Any successful observation of P350s must have in the 7–75 s period range (1) an amplitude greater than the noise level and (2) an amplitude greater than an absolute threshold fixed at 0.8% of the signal on the P-component. Our observations are split in two groups: group 1 includes our strongest observations for which amplitudes are greater than 1% of the signal on the P-component; group 2 shows intermediate signal amplitudes (falling in a 0.8–1% interval). The two groups are shown in Fig. 3a.

Modelling the low velocity layer. We model the layer assuming the same geometry as in ref. 2. The maximum shear-wave-velocity decrease in the middle of the layer is set to $\sim 0.2\,\mathrm{km\,s^{-1}}$ (−4% of IASP91). This value has been found to explain the amplitudes on Ps (refs 9,13), Sp (refs 2,12,13) and S-wave triplication[9] observations. The compressional velocity model is scaled using the IASP91 Vp/Vs ratio. We vary the vertical extension of the velocity gradient at the top of the layer (Fig. 2b). The top of the layer gives in the four period ranges (3–75 s; 5–75 s; 7–75 s; 10–75 s) a negative amplitude on the synthetic RFs (for example, in red in Fig. 2a), whose maximum is located in the middle of the downward negative-velocity gradient (Fig. 2b).

Received 5 July 2010; accepted 26 August 2010; published online 26 September 2010

References

1. Revenaugh, J. & Sipkin, S. Seismic evidence for silicate melt atop the 410-km discontinuity. *Nature* **369,** 474–476 (1994).
2. Vinnik, L. & Farra, V. Low velocity atop the 410-km discontinuity and mantle plumes. *Earth Planet. Sci. Lett.* **262,** 398–412 (2007).
3. Bercovici, D. & Karato, S. Whole mantle convection and transition-zone water filter. *Nature* **425,** 39–44 (2003).
4. Leahy, G. M. & Bercovici, D. On the dynamics of a hydrous melt layer above the transition zone. *J. Geophys. Res.* **112,** B07401 (2007).
5. Dasgupta, E. & Hirschmann, M. Melting in the Earth's deep upper mantle caused by carbon dioxide. *Nature* **440,** 659–662 (2006).
6. Wang, W. & Takahashi, E. Subsolidus and melting experiments of K-doped peridotite KLB-1 to 27 GPa: Its geophysical and geochemical implications. *J. Geophys. Res.* **105,** 2855–2868 (2000).
7. Suzuki, A. & Ohtani, E. Density of peridotite melts at high pressure. *Phys. Chem. Mineral.* **30,** 449–456 (2003).
8. Matsukage, K., Jing, Z. & Karato, S. Density of Hydrous silicate melt at the condition of Earth's deep upper mantle. *Nature* **438,** 488–491 (2005).
9. Song, T., Helmberger, D. & Grand, S. Low-velocity zone atop the 410-km seismic discontinuity in the northwestern United States. *Nature* **427,** 530–533 (2004).
10. Vinnik, L., Ren, Y., Stutzmann, E., Farra, V. & Kiselev, S. Observations of S410p and S350p at seismograph stations in California. *J. Geophys. Res.* **115,** B05303 (2010).
11. Schaeffer, A. J. & Bostock, M. G. A low-velocity zone atop the transition zone in Northwestern Canada. *J. Geophys. Res.* **115,** B06302 (2010).
12. Vinnik, L. & Farra, V. Subcratonic low-velocity layer and flood basalts. *Geophys. Res. Lett.* **29,** 1049–1052 (2002).
13. Vinnik, L., Kumar, M., Kind, R. & Farra, V. Super-deep low velocity layer beneath the Arabian plate. *Geophys. Res. Lett.* **30,** 1415–1418 (2003).
14. Fee, D. & Dueker, K. Mantle transition zone topography and structure beneath the Yellowstone hotspot. *Geophys. Res. Lett.* **31,** L18603 (2004).
15. Jasbinsek, J. & Dueker, K. Ubiquitous low-velocity layer atop the 410-km discontinuity in the northern Rocky Mountains. *Geochem. Geophys. Geosys.* **8,** Q10004 (2007).
16. Wittlinger, G. & Farra, V. Converted waves reveal a thick and layered tectosphere beneath the Kalahari super-craton. *Earth Planet. Sci. Lett.* **254,** 404–415 (2007).
17. Bagley, B., Courtier, A. & Revenaugh, J. Melting in the deep upper mantle oceanward of the Honshu slab. *Phys. Earth Planet. Inter.* **175,** 137–144 (2009).
18. Gao, W., Matzel, E. & Grand, S. Upper mantle structure beneath eastern Mexico determined from P and S waveform inversion and its implications. *J. Geophys. Res.* **111,** B08307 (2006).
19. Obayashi, M., Sugioka, H., Yoshimitsu, J. & Fukao, Y. High temperature anomalies oceanward of subducting slabs at the 410-km discontinuity. *Earth Planet. Sci. Lett.* **239,** 9–17 (2006).
20. Tauzin, B., Debayle, E. & Wittlinger, G. The mantle transition zone as seen by global Pds phases: No clear evidence for a thin transition zone beneath hotspots. *J. Geophys. Res.* **113,** B08309 (2008).
21. Kennett, B. L. N. & Engdahl, E. R. Travel times for global earthquake location and phase identification. *Geophys. J. Int.* **105,** 429–465 (1991).
22. Revenaugh, J. & Jordan, T. Mantle layering from ScS reverberations : 3. The upper mantle. *J. Geophys. Res.* **96,** 19781–19810 (1991).
23. Rychert, C. A. & Shearer, P. M. A global view of the lithosphere–asthenosphere boundary. *Science* **324,** 495–498 (2009).
24. Jordan, T. H. Global tectonic regionalization for seismological data analysis. *Bull. Seismol. Soc. Am.* **71,** 1131–1141 (1981).
25. Kohlstedt, D., Keppler, H. & Rubie, D. Solubility of water in the α, β and γ phases of $(Mg,Fe)_2SiO_4$. *Contrib. Mineral. Petrol.* **123,** 345–357 (1996).
26. Demouchy, S., Deloule, E., Frost, D. & Keppler, H. Pressure and temperature-dependence of water solubility in iron-free wadsleyite. *Am. Mineral.* **90,** 1048–1091 (2005).
27. Blackman, D. K. & Kendall, J. M. Sensitivity of teleseismic body waves to mineral texture and melt in the mantle beneath a mid-ocean ridge. *Phil. Trans. R. Soc. Lond.* **355,** 217–231 (1997).
28. Hier-Majumder, S., Ricard, Y. & Bercovici, D. Role of grain boundaries in magma migration and storage. *Earth Planet. Sci. Lett.* **248,** 735–749 (2006).
29. Debayle, E., Kennett, B. & Priestley, K. Global azimuthal seismic anisotropy and the unique plate-motion deformation of Australia. *Nature* **433,** 509–512 (2005).
30. Efron, B. & Tibshirani, R. Statistical data analysis in the computer age. *Science* **253,** 390–395 (1991).

Acknowledgements

Comments by David Bercovici, S-i. Karato, J. Trampert and Y. Ricard were very helpful to improve the first drafts of this manuscript. This work was supported by the French Young Researcher ANR TOMOGLOB no ANR-06-JCJC-0060 and the Dutch National Science Foundation under grant number NWO:VICI865.03.007. Computational resources were provided by the Netherlands Research Center for Integrated Solid Earth Science (ISES 3.2.5 High End Scientific Computation Resources) and the Institut de Physique du Globe de Strasbourg through the Beowolf computational resources. We thank the Iris and Geoscope data centres for providing seismological data.

Author contributions

B.T. designed the study and the numerical experiments, conducted the numerical experiments and the analysis of the seismic data and wrote the manuscript. E.D. contributed to the design of the numerical experiment and to the interpretation of the results and wrote the manuscript. G.W. developed some tools necessary to process the data and contributed to the design of the numerical experiment, the interpretation of the results and the preparation of the manuscript.

Additional information

The authors declare no competing financial interests. Supplementary information accompanies this paper on www.nature.com/naturegeoscience. Reprints and permissions information is available online at http://npg.nature.com/reprintsandpermissions. Correspondence and requests for materials should be addressed to B.T.